Autogenous self-healing of cement with expansive minerals-I: Impact in early age crack healing

Tanvir Qureshi[a*], Antonios Kanellopoulos[b] and Abir Al-Tabbaa[c]

[a] Department of Civil Engineering, University of Toronto, Toronto M5S 1A4, Ontario, Canada

[b] Department of Civil Engineering, School of Engineering & Technology, University of Hertfordshire, UK

[c] Department of Engineering, University of Cambridge, Trumpington Road, Cambridge CB2 1PZ, UK

ABSTRACT

This study investigates the impact of expansive minerals, namely magnesium oxide, bentonite clay, and quicklime on the early age autogenous self-healing capacity of Portland cement (PC) paste. Individual mineral dosage in PC was studied comprehensively together with several multiple mineral combinations. The study also covers a brief state of the art on autogenous self-healing and the use of minerals. The healing performance was compared using flexural strength recovery, crack sealing, and permeability tests. Materials microstructural investigations were carried out using XRD, TGA and SEM-EDX. The hydrated and swelling products of expansive minerals have effectively contributed to the production of healing materials. Cracks in the range of 150 µm healed efficiently in a mineral containing mixes within 28 days. Self-healing recovery was triggered through the crack bridging (strength recovery), sealing (physical closer of cracks through crystallisation) and durability performance improvement.

Keywords: Magnesium oxide (MgO), bentonite clay, quicklime, strength recovery, crack bridging, durability improvement, crystallisation.

1. Introduction

Portland cement (PC) concrete is an efficient, quasi-brittle, and heterogeneous material, which can withstand high compressive strength. Yet, concrete cracks due to mechanical actions, physicochemical phenomena and/or environmental weathering. Although traditional design codes do not consider microcracks (up to 0.4 mm) as an immediate threat to structural integrity [1], these

* Tanvir Qureshi. Tel.: +1(0)-416-978-5913; e-mail: tanvir.qureshi@utoronto.ca

cracks are undesirable. These cracks reduce concrete's toughness and increase permeability, which consequently leads to the compromise of concrete's durability and lifespan. Self-healing concrete could be a promising solution to mitigate these issues.

The concept of self-healing in cement-based materials is new, and progressed significantly in last two decades. Self-healing phenomenon in concrete was identified early in the mid-nineteenth century by Lauer and Slate [2] and the concept was gradually established by several researchers [3–7]. The healing processes in concrete are classified broadly into two principal groups, *autonomic* and *autogenous* healing [8]. In the former, healing agents are encapsulated into the concrete or composites. These encapsulated healing agents release by breaking the encapsulation (microvascular glass tube network [9–11] or microcapsule [12,13]) to repair the cracks. In contrast, *autogenous* self-healing is an intrinsic repairing process of cementitious material [4]. This inherent repairing occurs due to the hydration of remaining un-hydrated cement as well as carbonation of cement hydrates in the crack planes.

Compatible supplementary minerals can improve the self-healing capacity of traditional cementitious materials through increasing the formation of healing products. Depending on mineral types, it can serve either or both functionalities, i.e., to *remain considerably un-hydrated* after the initial mixing stage, and to *produce compatible expansive hydrated compounds* that can heal cracks. Potential minerals are required to remain substantially unhydrated after the initial concrete production. Then, a portion of primary hydration product and remaining unhydrated minerals are expected to contribute to the autogenous healing process. The formation of calcium carbonate in crack also plays a vital role in the healing process. Calcium carbonates form while primary cement hydration product calcium hydroxide in crack reacts with carbon dioxide in the atmosphere and dissolved in water. The crystallisation of calcium carbonate within the crack is considered as the primary mechanism for self-healing of matured concrete [5]. Table 1 summarises the published literature on the use of mineral additives for improving autogenous self-healing. Common minerals used by different researchers are calcium sulfoaluminate, lime, bentonite clay, fly ash (FA), silica fumes (SF), blast-furnace slag (BFS).

Table 1. Advancement in autogenous self-healing of cementitious materials with mineral additives.

Minerals	Composition	Damage type	Curing condition	Performance (healed crack width in time etc.)	Source
CSA, [a]H, [b]A, [c]L, Mont.	Up to 10% (concrete)	3PB, mechanical	water	-160-220 µm in 33d - Calcite, CASH	[18]
CSA	4.44% and 15.24% of cement (concrete)	tension force	still/continuous flow water	-100 µm –reduce flow - cont. flow is better	[19]
CSA, CA, [a]H, [b]A, [c]L, Mont.	PC with 10% CSA and 1.5% CA	Sp. tensile test	Water	-100-400 µm in 56 d -Calcite	[20]
Silica, [d]CEA, bentonite, CA	-8% individual -combination up to 14%	Compression, Sp. tensile	water, wet-dry, air, frizz-thaw	-220 µm in 2 weeks - [d]CEA (individually efficient) -silica, bent., CA (combination is efficient)	[21]
FA, SF, CA	OPC, OPC+30%FA, OPC+10%SF, OPC+1%CA	splitting tensile test	water	-50 µm in 12d - larger cracks heals efficiently with SF	[22]
FA	15 to 20% with PC (Paste)	shrinkage micro cracks	water	-meso-macro pores at 91, 182 and 364 d	[23]
FA	5 to 15% wt. of sand (concrete)	freeze-thaw	water	-Improve [e]DME over 90% in 28d	[24]
BFS	OPC+50% BFS	mechanical	water	-product formation is 3 times faster for CEM I	[17]
FA, slag	30-40% of cement (mortar)	shrinkage	water	-Improvement in compressive strength	[15]
[c]L, slag, FA	30, 50% FA; 50,75,85% slag (paste/mortar)	3PB, mechanical	water	-200 µm in 42d	[25]
slag	66% of cement (paste)	Sliced, mechanical	$Ca(OH)_2$ solution	-60% of 10 µm in 240 h - C-S-H, ettringite, hydrogenate etc.	[26]
Bentonite	nanoclay in mortar as internal water reservoir	mechanical	water	-enhanced hydration for self-healing	[27]
Bentonite, slag, [c]L	2% PVA by vol. Length=8mm, dia=40 µm	4PB	Water, wet-dry cycle, air	-naloclay improves the reloading deflection capacity	[28]
Quicklime, FA	(3%) on fly ash-PC cement pastes	mechanical	water	-Increased SiO_2 solubility - extra $Ca(OH)_2$	[29]
Expanded clay LWAs	Na-MFP and PC coated (Mortar)	mechanical	water	-absorption decrease - sodium, phosphorous and fluoride, CH	[30]
CSA	-PVA coated, up to 10% by wt. of cement (mortar,1:3)	3PB	water	- <100 µm -11d, - 100-200 µm -14d, - >200 µm-16d	[31]
CA: cement+sand +microsilica	1-2% of cement	4PB	water, open air	-60% cracks sealed under open air condition	[32]
MgO	4-12% of cement	drying shrinkage,3PB	water	- <500 µm in 28d - durability improved	[33]

Note: [a]H = hauyne, [b]A = anhydrite, [c]L = lime/limestone powder, [d]CEA = chemical expansive agent, 3/4PB = Three/four-point bending, OPC = Ordinary Portland cement, CASH= calcium aluminosilicate hydrate, CSA = Calcium sulfoaluminate, CA = crystalline additive, FA = Fly ash, SF= Silica fume, [e]DME = dynamic modulus of elasticity, LWAs = lightweight aggregates, Na-MFP = Sodium mono fluorophosphate (Na2FPO3, Na-MFP)

Smaller cracks (60 µm) in BFS and limestone powder containing fibre-reinforced cementitious composites healed efficiently due to the formation of $CaCO_3$ [14]. Another similar study reported the optimum healing performance of slag and fly ash based concrete with the mixing content of 30% and 40% with PC, respectively [15]. However, there is a maximum allowable crack width at a given slag

content and healing conditions, beyond which only partial healing is possible [16]. Olivier has investigated a BFS type as partial substitution of CEM I 52.5 PC cement for improving autogenous self-healing [17]. He found that 100% PC samples showed better self-healing performance than slag PC mix in the early healing periods (first 21 days). However, this performance alters in the case of PC with 50% BFS samples, thus resulting higher healing efficiency in later stages.

Tittelboom et al. [25] have compared the autogenous self-healing of individual and combination limestone, slag (BFS) and FA containing cementitious materials. The BFS and specifically FA showed negative influence in sealing efficiency, although both BFS and FA were expected to improve autogenous self-healing through remaining as a considerably unhydrated binder in the matrix. Then again, the strength and durability performance has improved, which can be attributed to the hydration of additive minerals inside crack planes.

Minerals such as FA, SF, and crystalline additive (CA) minerals were investigated by Jaroenratanapirom etal. for improving the self-healing of mortars [22]. Their proposed CA composed of 35.58% CaO, 16.81% SiO_2, 15.22% Na_2O, 1.98% Fe_2O_3, 1.93% Al_2O_3, and 1.29% MgO. Microcracks up to 50 μm were healed within 12 days, and wider cracks healed better with silica fume additives. Fourier Transform Infrared Spectroscopy (FT-IR) from their study confirmed that the formed healing materials were composed of calcium carbonate.

Exposure conditions also influence the concrete healing performance. Cracked concrete specimen cured under boiled water condition recovers mechanical strength with limited crack sealing performance [34]. While considering the influence of water flow in healing process, concrete with a Calcium sulfoaluminate (CSA) type expansive additive shows better healing performance under the continuous water flows than cured in stagnant water condition [19]. In a separate study, the replacement of 1% of cement content with active silica based CA sealed about 60% cracks under open air exposure condition [32,35]. Healing rate was reported faster initially (1 month) and continues slowly thereafter, and limited healing performance was observed without a continuous water supply.

The importance of water in the healing process is further addressed by Ferrara et.al. [36]. They used a specific CA for improving the self-healing properties of fibre reinforced concrete and studied the healing performance in different healing conditions (immersed, water contact, high humidity, and laboratory ambient). CA improved the durability of concrete in the immersed condition and resulted in an efficient sealing of ~250 μm cracks within 42 days. They also found that a crack sealing of over 70-80% is required for reasonable mechanical performance to be recovered. In this case, Ferrara et. al [36] reported stiffness recovery exceeding 20% in autogenously healed samples. The healing compounds formed by the crystalline admixture are similar to cement hydration products such as ettringite and calcium silicate hydrates. Although the healing performance of original concrete increases by this CA, a complete investigation is required to understand hydration mechanisms after concrete casting, as well as re-hydration kinetics and the carbonation of cement hydrates during the healing process.

Autogenous healing is also influenced by the marine environment [37,38]. In a laboratory scale mimic with seawater immersion, Ordinary Portland cement (OPC) mortar specimens show higher healing functionalities compared to BFS mortar specimens [37]. However, the situation reversed in fresh-water conditions. After 56 days data showed that about 100% of OPC and a BFS blended OPC samples in sea-water healed cracks up to 592 μm and 104 μm respectively, while this changed into 168 μm and 408 μm in the freshwater condition. It was found that the healing process is considerably influenced by the precipitation of brucite, i.e. $Mg(OH)_2$ and aragonite. In a similar study [38], the autogenous healing efficiency of OPC and BFS mortar samples was investigated in chloride, and a combination of chloride and sulphate solution to simulate a marine environment. While a chloride solution did not show much influence on the healing process, solutions with additional magnesium sulphate improve the sealing of cracks forming brucite layers at the crack planes. Therefore, the compositions of cement matrix such as specific supplementary cementitious materials and healing environment have a significant influence on the autogenous healing process.

It was found that the expansive minerals as supplementary cementitious materials improve the autogenous self-healing capacity of PC concrete. Minerals optimum expansive action promote the

formation of efficient hydration products, which not only can seal but also heal the cracks [18,33,39–43]. The current study aims to investigate the autogenous healing performance of cement paste with three different expansive minerals (MgO, bentonite and quicklime) under continuous water immersion. Findings of this study are presented in two parts. The first part (Part-I), herein this paper, presents the early age self-healing performances of cement past composition with minerals at a constant standard consistency limit. Second part (Part-II) paper covers the optimisation of mineral mix composition in PC and correlates the impact of hardened cement paste age at crack formation with the healing process. In Part-II, the water to cement ratio was constant, while the workability was adjusted using the water reducing admixtures.

2. Materials and methods

2.1 Materials

Table 2 presents the chemical and physical properties of PC and minerals.

Table 2. Chemical and Physical properties of PC, MgO, bentonite, and quicklime.

	PC: CEM I 52.5 N	MgO (M)	Bentonite Clay (B)	Quicklime (L)
Chemical Property				
SiO_2 (%)	19.50	2.25	54.20	0.80
Al_2O_3 (%)	4.90	0.22	18.80	0.10
CaO(%)	63.60	0.87	4.90	93.90
Fe_2O_3(%)	3.10	0.53	5.00	0.06
MgO(%)	0.90	93.18	3.70	0.50
SO_3(%)	3.30	--	--	0.03
Na_2O(%)	--	--	3.00	--
K_2O(%)	--	--	0.60	--
TiO_2	--	--	0.70	--
$CaCO_3$	--	--	--	4.00
LOI(%)-Loss on ignition	2.10	2.59	--	--
Physical properties				
Avg. Particle Size (µm)	5.00-30.00	30-40*	4.75-75	53
Density (g/cm^3)	3.16	3.02*	2.80	3.34
S. Surface area (m^2/g)	0.30-0.40	16-20*	0.48	--
Bulk density (g/cm^3)	0.90-1.50	--	--	0.84-1.02
Reactivity	--	145 Seconds	--	49 Seconds

Note: * Properties collected from reference [44].

Portland cement type CEM 1 52.5 N satisfying BS EN 197-1 [45], was supplied by Hanson, UK. RBH Ltd, China supplied moderate reactive grade magnesia (MgO 92/200). Bentonite was supplied by Kentish minerals and Quicklime (Calbux) satisfying BS EN 459-1:2001[46] was supplied by Tarmac Buxton Lime and Cement, UK. The reactivity of MgO and quicklime were measured using an accelerated reactivity test (as described in [47]) and a digital pH meter was adjusted in the experimental setup (as described by [48]). Fig. 1 illustrates the XRD diffractograms of pure minerals used in this experiment. Each XRD graph characteristic peaks corresponds to associated minerals.

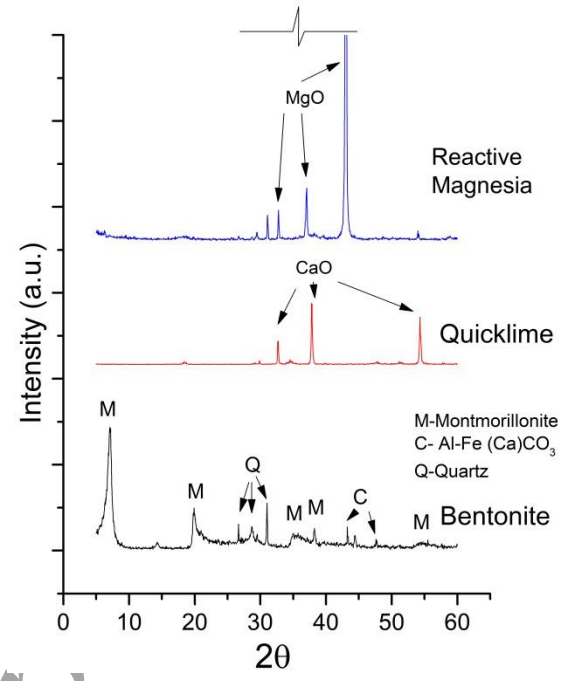

Fig. 1. The XRD of magnesia (MgO), quicklime, and bentonite used in this experiment.

2.2 Sample preparation and curing

Table 3 presents the mix designs used in this study. The CON (PC100) was the reference control 100% PC paste without additives, while the rest of the mixtures contained different percentages of minerals as PC supplements. Tap water was used to prepare the cement paste. The standard consistency limit of mixes following ASTM C 187 [49] was used to determine water to cement ratio. This constant consistency limit allowed comparing the healing performance of different cement-mineral mix composition at the same workability condition.

The mixes were cast and finished as prescribed at BS EN 196-1:2005 [50] and left to set for 24 hours. A planetary type mixer was used in the mixing process. Cube samples (40mm x 40mm x 40 mm) were prepared for the compressive strength test. Prism samples (40mm x 40mm x 160mm) were prepared for crack forming through a three-point bend test and investigating their corresponding healing performance. A flexible steel wire (40 mm long and ~1 mm diameter) was placed at 2.5 mm below the top loading surface to avoid complete collapse of the sample during the test. Disks 50 mm diameter and 15 mm thick were prepared for gas permeability tests. All samples were then cured under water at 20±1 ^{o}C in desirable periods as described in the corresponding experimental method at section 2.3 and 2.4.

Table 3. Cement mix compositions by percentage weight.

	Mix	PC (PC)	MgO (M)	Bentonite (B)	Quicklime (L)	Water
Individual minerals	CON (PC100)	100	-	-	-	28.5
	PC97.5M2.5	97.5	2.5	-	-	29.2
	PC95M5	95	5	-	-	30
	PC90M10	90	10	-	-	33
	PC97.5B2.5	97.5	-	2.5	-	30.3
	PC95B5	95	-	5	-	32
	PC90B10	90	-	10	-	35.5
	PC97.5L2.5	97.5	-	-	2.5	29.5
	PC95L5	95	-	-	5	30.5
	PC90L10	90	-	-	10	32.5
Combination minerals	PC90M5B5	90	5	5	-	33.5
	PC85M10B5	85	10	5	-	35
	PC90M5L5	90	5	-	5	32
	PC85M10L5	85	10	-	5	33
	PC85M5B5L5	85	5	5	5	35.5
	PC80M10B5L5	80	10	5	5	36

2.3 Compressive strength test

Compressive strength was measured following BS EN 196-1:2005 [50]. Cube samples were cured under water and compressive strength was measured at 1, 14 and 28 days.

2.4 Evaluation of the self-healing performance

Healing performance was studied by using visual observations of crack sealing, strength recovery and durability improvement as indicated by the gas permeability test. Prism and disc samples were cracked at one day (24hr) after casting, and their healing was investigated up to 28 days.

2.4.1 Crack sealing efficiency evaluation

Cracked prisms were marked along the crack path (at least two spots at the bottom and one spot on both sides). Prism samples were cracked using three-point bend test according to BS EN 12390-5 [51] and ASTM: D790-10 [52]. Prior to cracking, all specimens were notched (depth 1.5 mm and width 2.0 mm) with a rotating diamond blade. Preceding testing, a clip gauge was attached close to the notch edges to monitor crack mouth opening displacement (CMOD) as presented in Fig.2a. The prisms were loaded over a span of 120 mm and at a rate of 0.125 mm/min. Loading was stopped when the crack opening reached 0.30 mm. Upon the removal of the load, specimens had a bottom residual crack width in average 0.18±0.04 mm, while few samples split completely only holded by the flexible wire at top surface. However, six prisms were cast for each mix type to have at least three prims in desirable damage state after the three-point bend test. The widths and corresponding cross-sectional areas of those marked places were observed after the initial cracking and at different recovery periods (initial cracking-0 day, and 7 days, 14 days and 28 days). Digital images were taken using a GXCAM 1.3 type digital stereo microscope (GT Vision Ltd.). Finally, the crack area from the image was measured using Image-J software and the crack sealing efficiency CA (%) over time was calculated using equation 1:

$$CA(\%) = \frac{CA_0 - CA_t}{CA_0} \times 100 \qquad (1)$$

where CA_0 is the crack cross-section area just after cracking, and CA_t is the crack cross-section area after healing in time t.

2.4.2 Strength recovery

Flexural stress and strain were calculated using equations 2 and 3 below.

$$\sigma_f = \frac{3PL}{2bd^2} \quad (2)$$

$$\varepsilon_f = \frac{6Dd}{L^2} \quad (3)$$

Where, σ_f is stress in the outer surface at the midpoint (MPa), ε_f is the strain in the outer surface (mm/mm), P is the load (N), L is the support span (mm), b is the width (mm), d is the depth (mm), and D is the maximum deflection of the prism centre (mm). Prisms were reloaded again after healing up to 14 and 28 days and the strength recovery (SR) were then measured using Equation 4.

$$SR(\%) = \frac{rec,\sigma_{f,\max}}{ini,\sigma_{f,\max}} X100\% \quad (4)$$

In this equation, *SR* is the percentage of flexural strength recovery; $rec,\ \sigma_{f,\ max}$ is the maximum flexural strength recovered at the testing time (after 14 and 28 days); and $ini,\ \sigma_{f,\ max}$ is the maximum flexural strength in initial cracking (cracking of 1 day sample).

2.4.3 Coefficient of gas permeability

A liquid methanol gas source based technique was used to evaluate the gas permeability coefficient as described in [12,53]. The experimental setup of the gas permeability is presented in Fig. 2b. One day aged cement paste discs for gas permeability test were cracked under crack mouth opening control mode using an Instron machine and a clip gauge. Cracked discs were left to cure under water for another 28 days. Samples were then dried for 72 hours to remove moisture and fixed with epoxy sealant at the top of the glass pressure cells containing methanol, which were immersed in a 40^{o}C water bath (Fig. 2b). The mass loss with time was recorded at predefined time intervals until a steady-state loss was reached. Further description of this experiment can be found in [33], which explains how to measure the intrinsic permeability coefficient (k) from the gas permeability test results.

(a) (b)

Fig. 2. Experimental setup: (a) Three-point bend test, and (b) Gas permeability.

2.5 Microstructural investigation

The microstructure of cement paste and healing compounds were investigated using: thermogravimetric analysis (TGA) through Mettler Toledo TGA/DSC-1 in 50-1000 ^{0}C temperature range at a rate of 10 ^{0}C/min in nitrogen (50 ml/min) environment with ~20 mg of dried powdered samples; a mid-range Fourier transformed infrared (FT-IR) in 4000-525 cm^{-1} by a Spectrum 100 spectrometer (Perkin Eimer); X-ray diffraction (XRD) by Siemens D500X ray diffractometer in a range of 5-60^{o} of 2Θ at a rate of 2 s/step and scanning resolution of 0.05^{o}/step; and a high definition scanning electron microscope (SEM) image and energy dispersive x-ray (EDX) by Nova nono SEM 450. The EDX detector was a Bruker QUANTAX EDX, Xflash 6|100 detector type.

Powder samples were used to perform the TGA, XRD and FT-IR tests. Initial cement samples were collected after 24 hr casting, from the debris of crushed 40 mm cubes in compression test. Self-healing materials were obtained from prisms following the final loading of the specimens to failure after 28-days recovery. Healing materials were extracted carefully from the healed cracked planes using a file and a scaler tool. Initially, samples were treated with acetone for three days to suspend hydration. Samples were then dried in a vacuum desiccator for four days and oven dried for another three days at 60^{o}C. Finally, samples were grinded to pass a 75 µm mesh sieve and collected for the test.

Self-healing materials for SEM and EDX were collected cautiously in small pieces, and care was taken so that healed plane remained intact. The rest of the steps were same as XRD sample preparation except for the grinding of samples prior preserving in a desiccator. Samples were then gold coated using a K550 Emitech coating machine to ensure suitable conductivity for microscopy and EDX. The microscope was operated at an accelerating voltage of 15 keV with a working distance of ~6-8 mm and the time of EDX analysis per point was 60 s with ZAF correction using a built-in machine software.

3. Results and discussion

3.1 Compressive strength development

The compressive strength of mixes at 1, 7 and 28 days is illustrated in Fig. 3. Compressive strength gradually increased in all mixes over time. Compared to CON (PC100), the substitution of 5% MgO has no impact on compressive strength at 28 days, whereas substitution of 5% bentonite and quicklime reduced ~7% and ~22% compressive strength, respectively. However, increasing the mineral substitution amount to 10% caused a considerable reduction in the measured compressive strength at all ages. At 28 days, PC90M10, PC90B10, and PC90L10 mixes resulted in about 14%, 40% and 20% reduction in compressive strength, respectively, compared to PC100. Combined minerals had a combined impact on compressive strength (Fig. 3b).

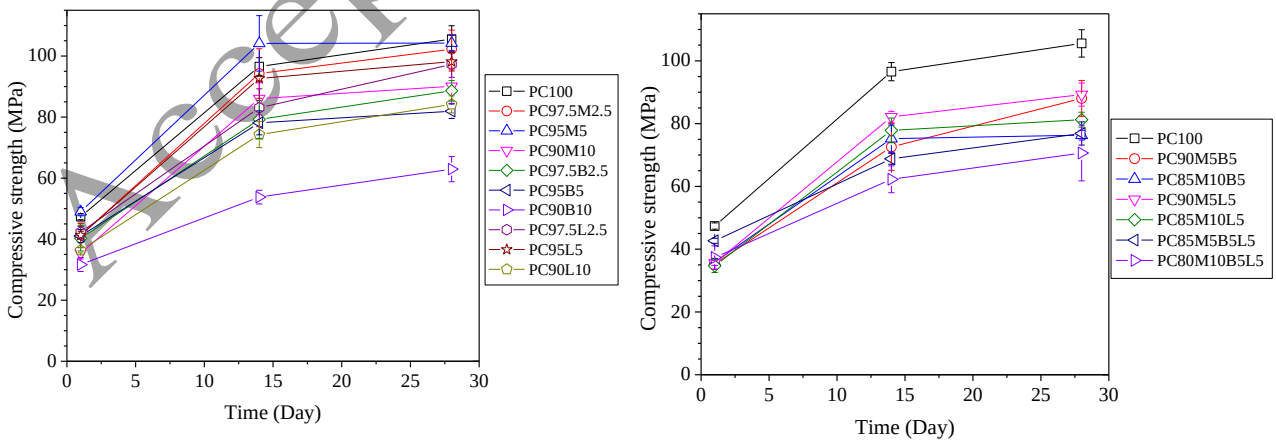

(a) (b)

Fig. 3. Compressive strength development, (a) individual mineral substitution mixes, and (b) mineral combination mixes.

MgO up to 5% slightly improves the 14 days compressive strength of PC95M5 mix compared to PC100 due to its chemical properties. The primary hydration product of MgO is brucite, i.e., $Mg(OH)_2$, one of the highly compatible cement hydration products which trigger expansion in the matrix [54]. Optimum proportions of MgO in the cement mix produced efficient internal stress inside the cement matrix which balances the shrinkage stress and results in a positive impact on strength development. Besides that, unconsumed MgO acts as a filler material in the microstructure [48], which compacted the paste matrix and improve strength properties. Quicklime, on the other hand, produces $Ca(OH)_2$ as an initial hydration product. Although higher proportions of $Ca(OH)_2$ in the cement matrix have the potential to improve autogenous self-healing capacity, the presence of more than optimum proportions results in a little decrease in compressive strength development compared to PC100. Unlike MgO and quicklime, bentonite drastically reduces compressive strength due to its more water-absorbing nature and lower participation in the pozzolanic reaction of cement. Bentonite instead acts like filler and water absorber which negatively affects the strength development of PC blends.

3.2 Impact of minerals on self-healing properties

3.2.1 Crack sealing efficiency

The cracks occurred near the surface was hydrated and carbonated with the availability of air and water, then sealed up tight in the outer zone. The crack sealing was typically visualised in the crack tip. Different types of healing materials were formed at different crack depths (Fig. 4). The inner core section of the cracks was mostly hydrated then limitedly carbonated compared to the outer periphery zone. Fig. 5 shows a typical crack closures pattern in PC100 and mineral containing (e.g. PC95M5) samples. It can be noted that expansive mineral containing samples show much efficient sealing compared to PC100 samples. Effective sealing can cause the reduction of water passing through the cracks, which was similarly reported in the literature [13,18]. Samples with expansive minerals were mostly sealed within 14 days, and higher content of expansive mineral in the mixes showed higher sealing nature.

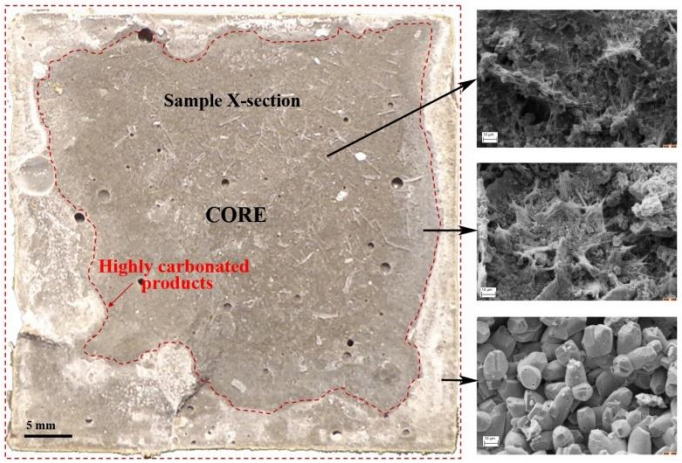

Fig. 0. Healing material formation pattern in a typical prism crack plane *(left)*, corresponding location SEM image at 2000 x magnification *(right)*.

The crack sealing efficiency (CA%) following Equation 1 is presented in Fig. 6. Sealing efficiency showed increasing trend over time. Average cracks in the bottom of the prisms were 0.18±0.04 mm. Smaller cracks sealed faster than the wider once. After 28 days recovery, crack sealing efficiency was over 95% for PC90M5B5 followed by around 85% for PC95B5, PC95L5, and PC80M10B5L5, compared to the PC100 samples 56% efficiency. Bentonite and quicklime showed slightly better sealing property compared to MgO individually. Nonetheless, combined minerals resulted in improved sealing efficiency in the most of the cement mixes.

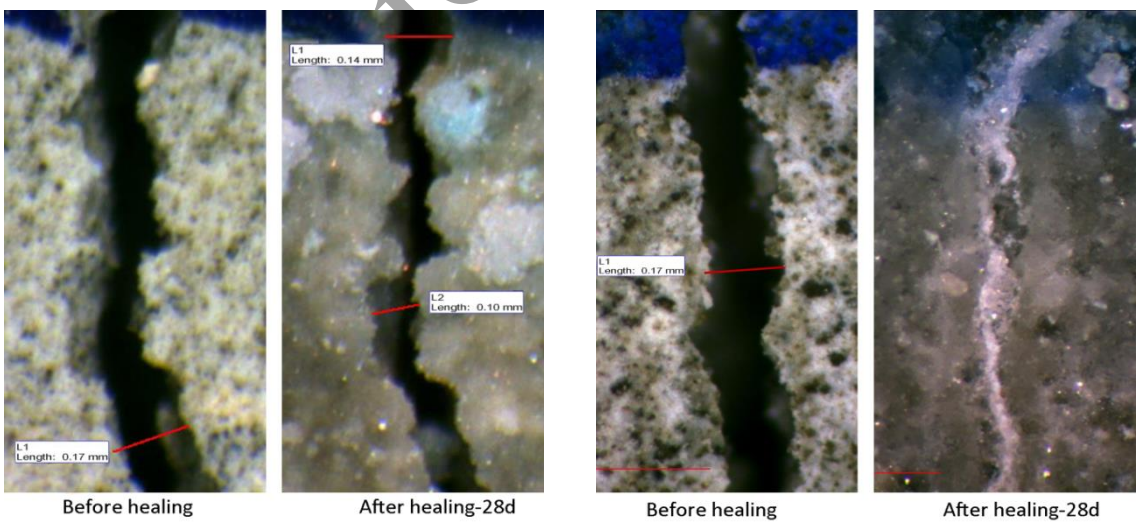

(a) (b)

Fig. 5. The typical crack sealing pattern in 28 days: (a) CON (PC100), and (b) Cement with expansive minerals.

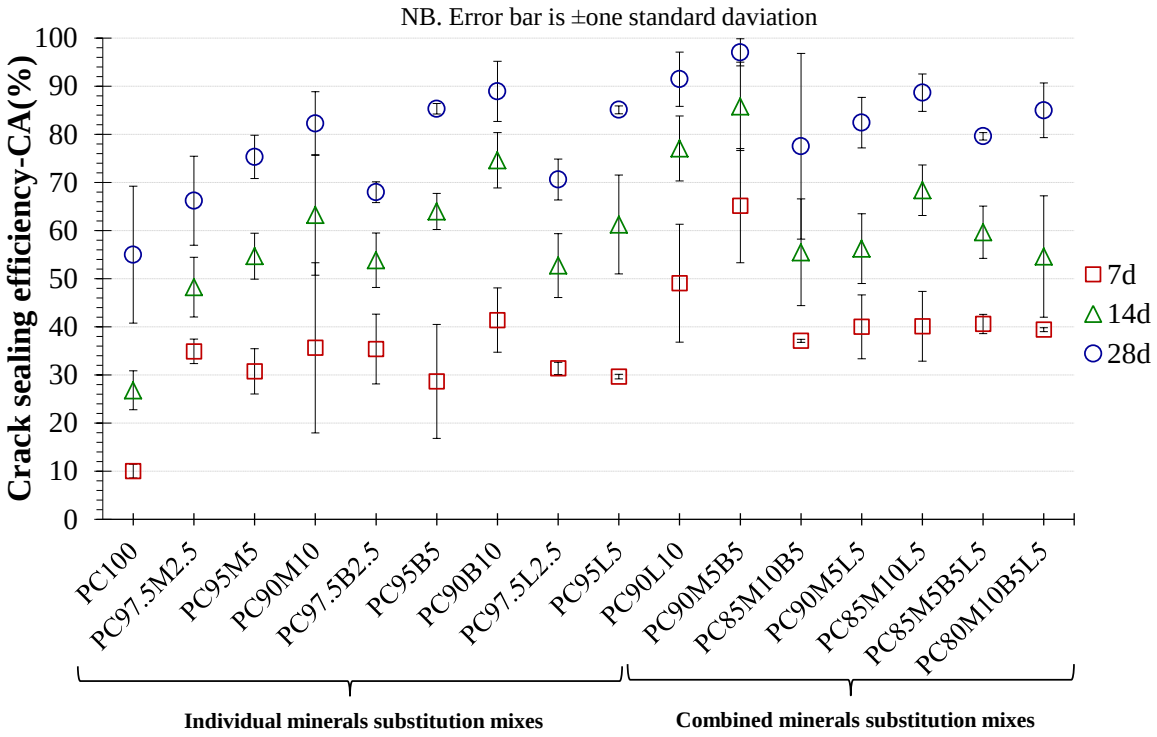

Fig. 6. The crack sealing efficiency-CA(%) of different mixes.

3.2.2 Strength recovery

Flexural strength recovery from three-point bend test using Equation 4 is considered as the mechanical strength recovery parameter. Although the incorporation of higher mineral proportions was found to reduce the compressive strength to some extent (Fig. 3), this compensates for an increase in self-healing performance in most cases. The strength recovery results are presented in Fig. 7. All individual minerals substitutions up to 5% showed maximum strength recovery. Overall the strength recovery shows increasing trend from 14 days to 28 days in all mixes. Although a higher proportion of individual minerals increased crack sealing, strength recovery performance was reversed from 5% to 10% substitution mixes. Since there was no reinforcement in these cement paste prisms to restrain crack, excessive expansion of matrix without restraint might cause a negative impact on crack bridging and limits strength recovery. The healing performances of PC with high content of expansive minerals may be beneficial in cases where the crack width is restrained with fibres or reinforcements or even with the help of external pressure conditions to contain expansive healing products [55]. Overall, MgO showed higher recovery performance followed by quicklime and the least with bentonite.

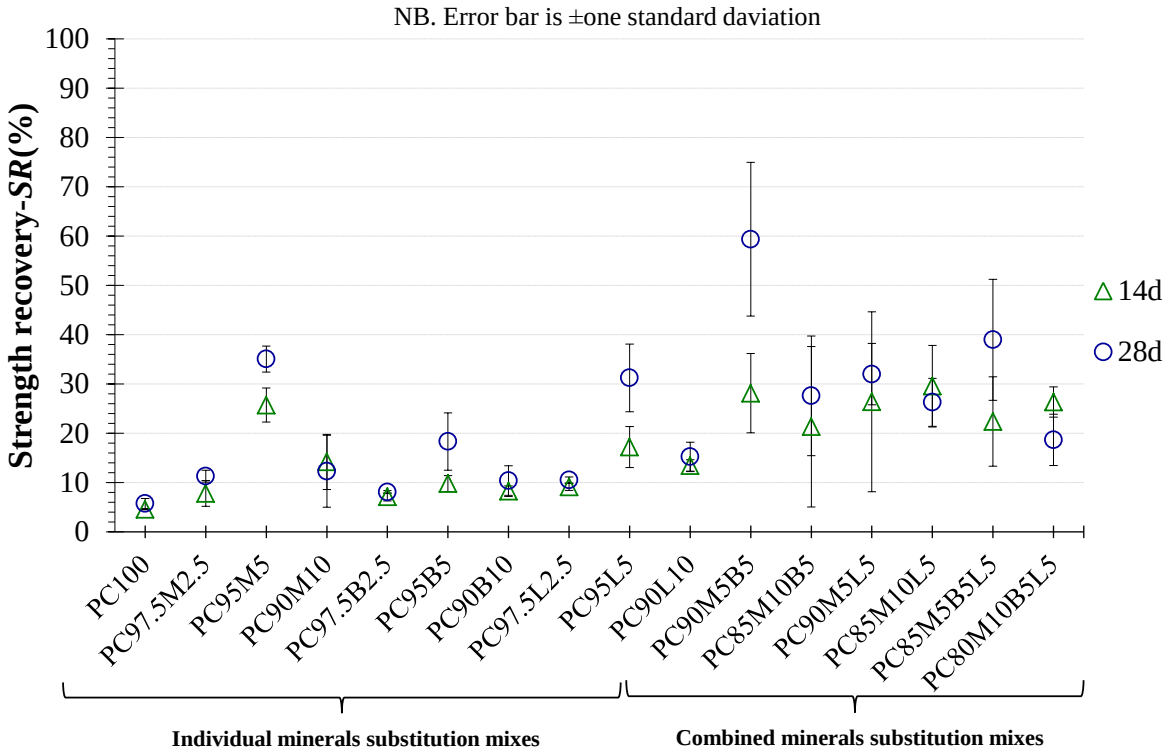

Fig. 7. Flexural strength recovery -SR(%) of mixes in 14 and 28 days.

The combination of minerals results in higher strength recovery than individual substitutions. This is somewhat similar to the crack sealing performances. Magnesium oxide shows good compatibility with bentonite and quicklime. The strength recovery of PC100 was only 4% and 6% at 14 days and 28 days, whereas it was nearly 28% and 60% for the PC90M5B5 specimens. Lower average crack width (~150µm) of PC90M5B5 showed a positive impact on strength recovery performances. Quicklime also demonstrated a positive influence with MgO and bentonite. As found in PC85M5B5L5, strength recovery increased to around 40% in 28 days. One of the possibilities is that the healing may have occurred in deeper crack planes rather than only being superficial in those mixes. So far, the most efficient strength recovery ranged between 5% cement replacement of each mineral mixes (PC85M5B5L5) and 5% of both MgO and bentonite mixes (PC90M5B5).

3.2.3 Gas permeability

Gas permeability is considered as an indicator of durability performance improvement after healing. Fig. 8a shows the gas permeability coefficients of different mixes after 28 days healing. In the graph, PC100-un cracked and PC100-cracked represented un-cracked and cracked PC100 discs respectively. PC100 un-cracked discs showed about 89% reduced coefficient values compared to PC100 cracked healed discs. Overall, MgO samples resulted in considerable permeability reduction compared to PC100-cracked samples followed by quicklime and bentonite mixes. Then again, individually 5% MgO samples showed the least permeability. The bentonite and quicklime samples showed a gradual reduction in the permeability with the increasing proportions of substitution in the mix. Combination mixes showed reduced permeability performance except for the highest substitution mix PC80M10B5L5. Little higher permeability in the PC80M10B5L5 mix may be attributed to the excessive expansive nature of the mix. Besides, excessive amount of expansive minerals may have adverse effect on the durability performance of that cement based concrete. Permeability in the combination mixes almost follows the trend of MgO 5% and 10% mixes. The reduction of permeability coefficient compared to PC100-cracked varied from around 70% for PC90M5B5, PC85M10L5 and PC85M5B5L5 followed by other combination mixes, and then individual MgO, bentonite and quicklime PC mixes.

Fig. 8b presents the correlation between crack sealing and gas permeability recovery as well as between crack sealing and strength recovery. The trend line shows increasing strength recovery and decreasing permeability coefficient with the increasing crack sealing, although there are anomalies out of the trend line due to different crack tip sealing mechanisms. While the higher expansive nature of some mixes showed effective crack sealing, corresponding strength recovery was not always promising. As noted, strength recovery trend was not the same as crack sealing performance in 10% individual substitution mixes and PC80M10B5L5. The crack tip in those mixes may sealed in faster rate which might have restricted the further penetration of water and dissolved CO_2 in depth for continuous rehydration and carbonation required for efficient healing. A similar phenomenon was described in [20] that erstwhile the highly and faster crystal producing nature of cementitious

materials might have resulted in a thin layers of crack tip closing compounds restricting hydration. This also explains the anomalies that are less noted in crack sealing versus permeability coefficient trend compared to crack sealing verses strength recovery trend.

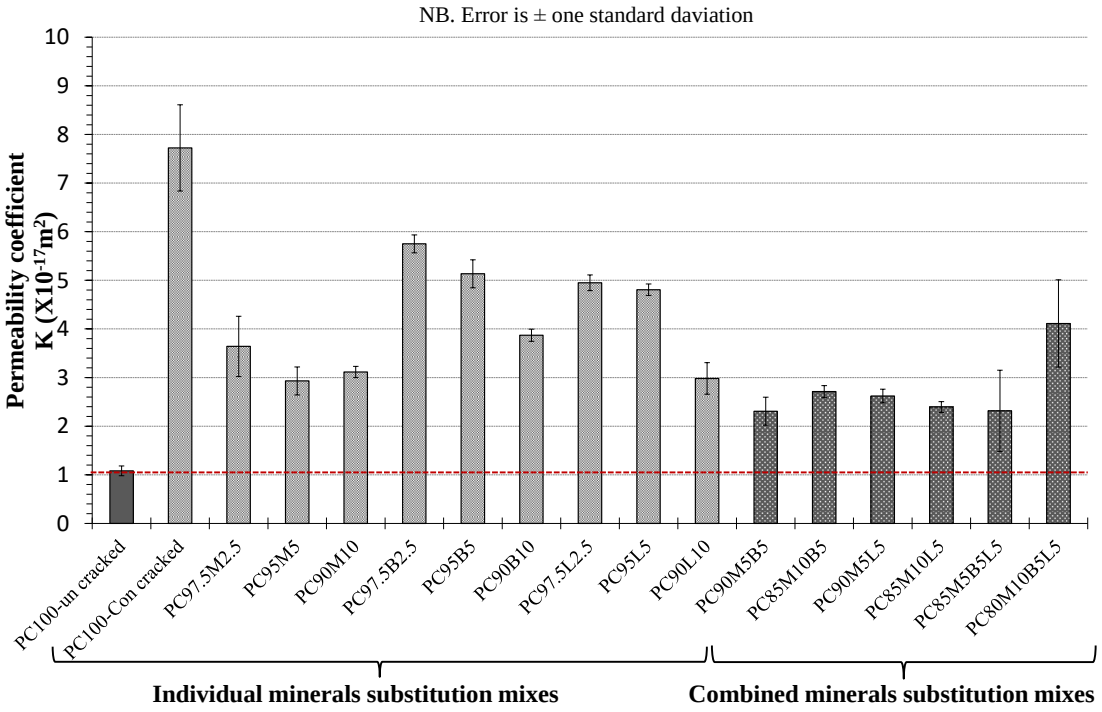

(a)

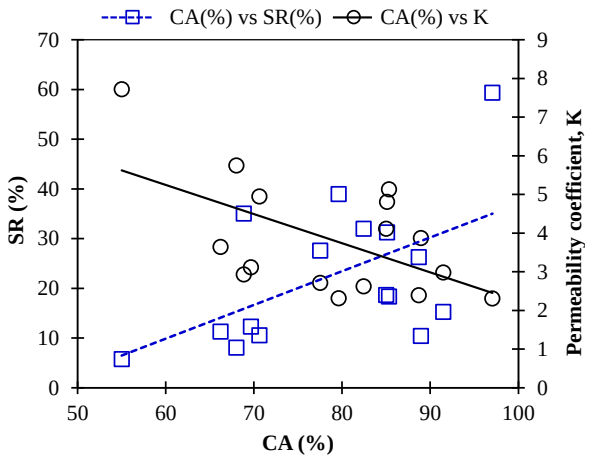

(b)

Fig. 8. (a) Gas permeability coefficients of hardened cement paste discs after 28-day healing. (b) crack sealing efficiency (CA%) correlation with gas permeability coefficient (K) and strength recovery (SR %).

The durability improvement due to self-healing is a good indicator of healing, and these permeability results are in agreement with the results of crack sealing and strength recovery. High strength recovery and moderate rate of crack sealing might allow efficient healing inside the crack plane avoiding only sealing in the crack tip. This phenomenon was most common in 5% MgO mixes.

Healing performances were higher in the mineral-containing cement mixes compared to PC100 mix despite their higher water/binder ratio. This is an interesting finding since the unhydrated cementitious materials contents were expected to be lower with higher w/b ratio. Therefore, substituted minerals remained considerably unhydrated even in the higher w/b ratio, which positively triggered the healing process. To better understand the entire healing process, the microstructural investigations of materials were undertaken, and are presented in the following sections.

3.3 Microstructure of the initial cement paste

The microstructural investigation of initial, i.e. one (1) day aged cement mixes have been carried out using XRD and TGA. This was conducted to understand the state of hardened cement pastes at the time of cracking and initiation of healing in immersed condition.

3.3.1 XRD of initial mixes

The XRD patterns (Fig. 9) of initial cement mixes showed similar features in the main cement hydration phases (portlandite, ettringite, calcite, anhydrite) and unhydrated phases (C_2S, C_3S). MgO mixes showed the peak of major hydration product $Mg(OH)_2$ (brucite). It was noted that the intensity of unhydrated MgO and anhydrites peaks showed an increasing trend with the increasing proportions of MgO content (eg. PC97.5M2.5 to PC90M10 in Fig. 9a). The major unhydrated MgO peak around ~43^o was distinctly correlating to the amount added in the mixes. Similarly, quicklime elucidated the corresponding increment in the portlandite and unhydrated CaO peaks (e.g. PC95L5, PC85M5B5L5). The presence of anhydrite was noted, which may have enhanced the rehydration capacity of mixes. Anhydrite phase was reported to consume through hydration by increasing the compressive strength in later stages [56]. These remaining unhydrated C_2S, C_3S, MgO and CaO together with higher proportions of brucite, anhydrite and portlandite phases were crucial in the healing process.

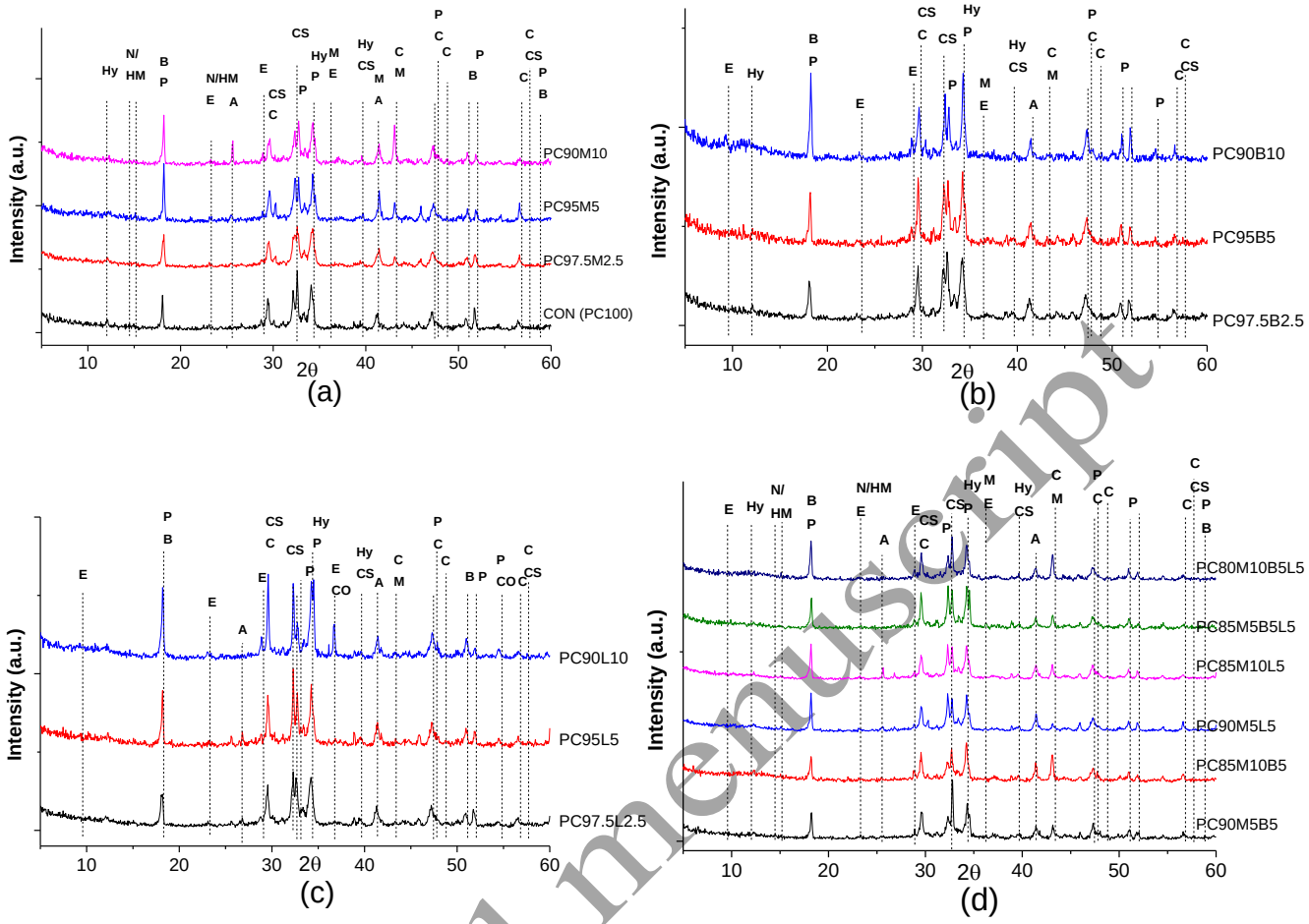

Fig. 9. X-ray diffraction diagrams of initial cement mixes after 24 hr of casting , (a) CON (PC100) and MgO-mixes, (b) bentonite-mixes, (c) Lime-mixes, and (d) combination mixes (Graph notations: E= Ettringite, A= Anhydrite, Hy= Hydrotalcite, N/HM= Nesquehonite/Hydromagnesite, B=Brucite, C= Calcite, CS= C_2S and C_3S, P= Portlandite, M=MgO/$MgCO_3$).

3.3.2 TGA of initial mixes

Fig. 10 presents the TGA results of initial cement mixes, i.e. after 24 hrs from casting. Various TGA decomposition peaks in all mixes were overlapping as similarly evident in XRD diagrams (Fig. 9). The overlapping of hydrated phases may have resulted intense peaks in TGA. The endotherms and their corresponding mass losses in Fig. 10 were similar to others study [56–59] and ascribed to C-S-H gel ~150^{o}C [57]; Aluminium, ferric oxide, mono-sulphate (Afm phase) and gehlenite hydrate ~ 200^{o}C; portlandite (Calcium hydroxide: CH) 425-550^{o}C [58], ettringite ~68^{o}C, brucite ~350^{o}C[59],

calcite ~640–670°C [56] and different carbonate phases ~700^{o}C. The DTG curve indicated all these hydration peaks similarly presents in individual mineral substitution mixes (Fig. 10a-c) and combination mineral substitution mixes (Fig. 10d).

A quantification of TGA weight loss (non-evaporative water loss) percentage between three major ranges associated to brucite: 300 – 400^{o}C, CH: 400 – 500^{o}C, and carbonate phases (CP): 600 – 750^{o}C, was measured and presented in Fig. 10e. Calcium hydroxide (CH) is the primary crystalline products of the hydration reactions of dicalcium and tricalcium silicates (C_2S and C_3S) of PC, and quicklime. Quicklime individually and in combination with MgO show increasing trend of CH production. This confirms high reactivity of quicklime at an early age of cement hydration. A slight indication of brucite peak is noted with the increasing proportions of MgO (Fig. 10a and 10d). However, corresponding peak and weight loss were much lower compared to C-S-H, ettringite, portlandite and carbonate phases. The quantification of weight loss percentage suggests that brucite production is not much influenced in initial mix with MgO substitution compared to PC100. The impact of individual bentonite entrapped water could not be separated since this overlaps with ettringite phase and carbonate phases peaks. However, bentonite in combination with MgO shows increasing brucite formation which results in about 1.03% weight loss for brucite phase in PC85M10B5 compared to that of 0.80% weight loss in PC100. Therefore, MgO considerably remained unhydrated in the initial cement mixes, although bentonite encourages little proportions of MgO nucleation to produce brucite. The high proportion of expansive mineral substitution in M80M10B5L5 increases hydration products, in particular, weight loss percentage for calcite increased to 3.39% compared to 2.93% in PC100. Overall the weight loss variation in all mixes due to the addition of expansive minerals is not extensive, although there is a slight indication of brucite peak in MgO mixes and minor deviation in carbonate phases due to the addition of quicklime and bentonite. Hence, a considerable proportion of substitution minerals remained unhydrated in the matrix, which was expected to improve the healing process.

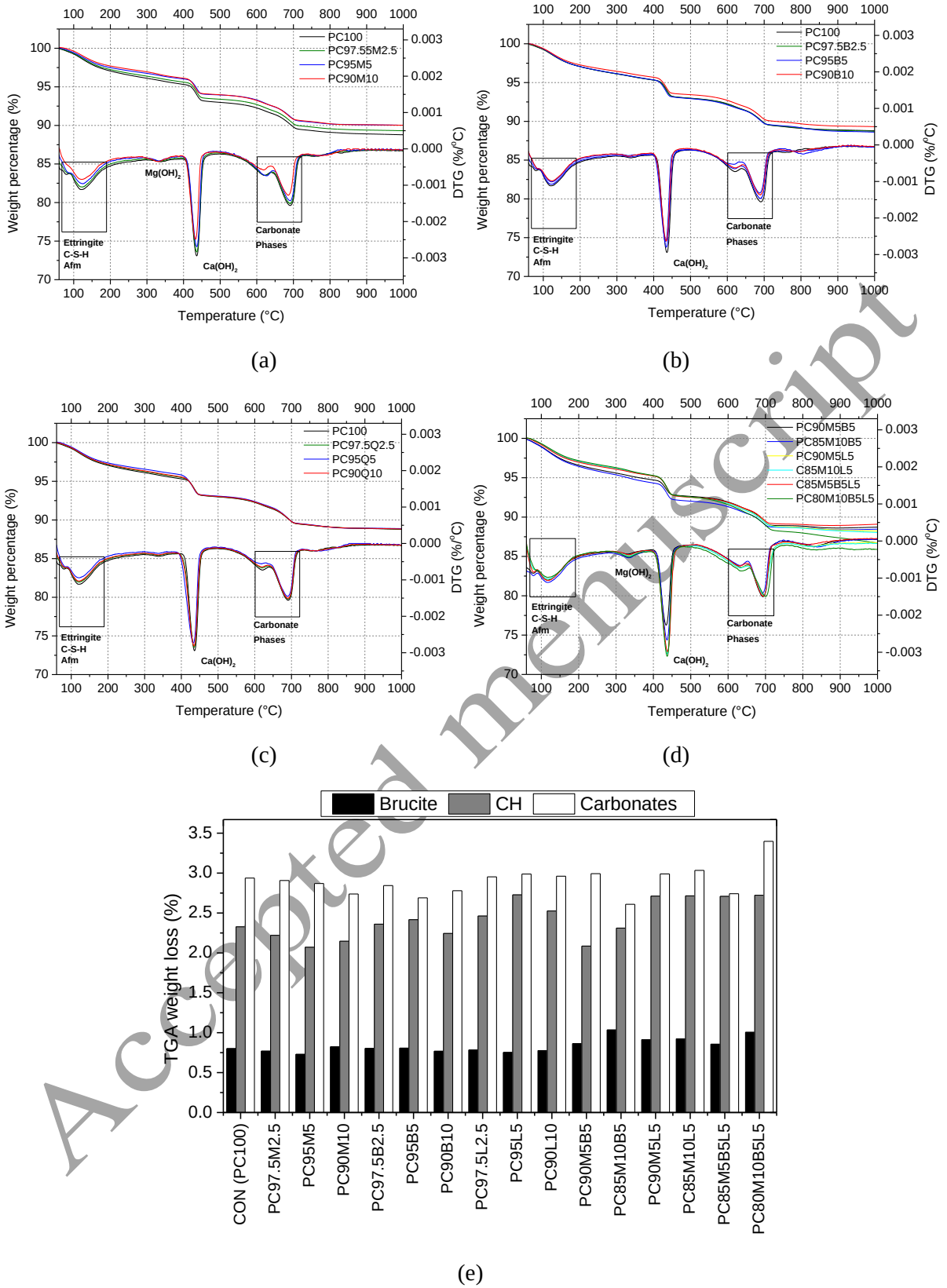

Fig. 10. TGA analysis of initial mixes after 24 hr of casting, (a) CON and MgO-mixes, (b) CON and bentonite-mixes, (c) CON and Lime-mixes, (d) combination mixes, and (e) TGA weight loss (%) for brucite, CH, and carbonate phases.

3.4 Microstructure of the self-healing materials

This section depicts the influence of expansive minerals on the microstructure of healing product formation and the recovery mechanism.

3.4.1 XRD of healing materials

The XRD analysis on healing compounds is shown in Fig. 11. Several common PC hydration products were noted in the XRD graphs (Fig. 11). The XRD spectrum indicated that principal healing materials were carbonates and cementing hydrated products. In particular, calcite, portlandite, ettringite, and brucite were ientified dominantly.

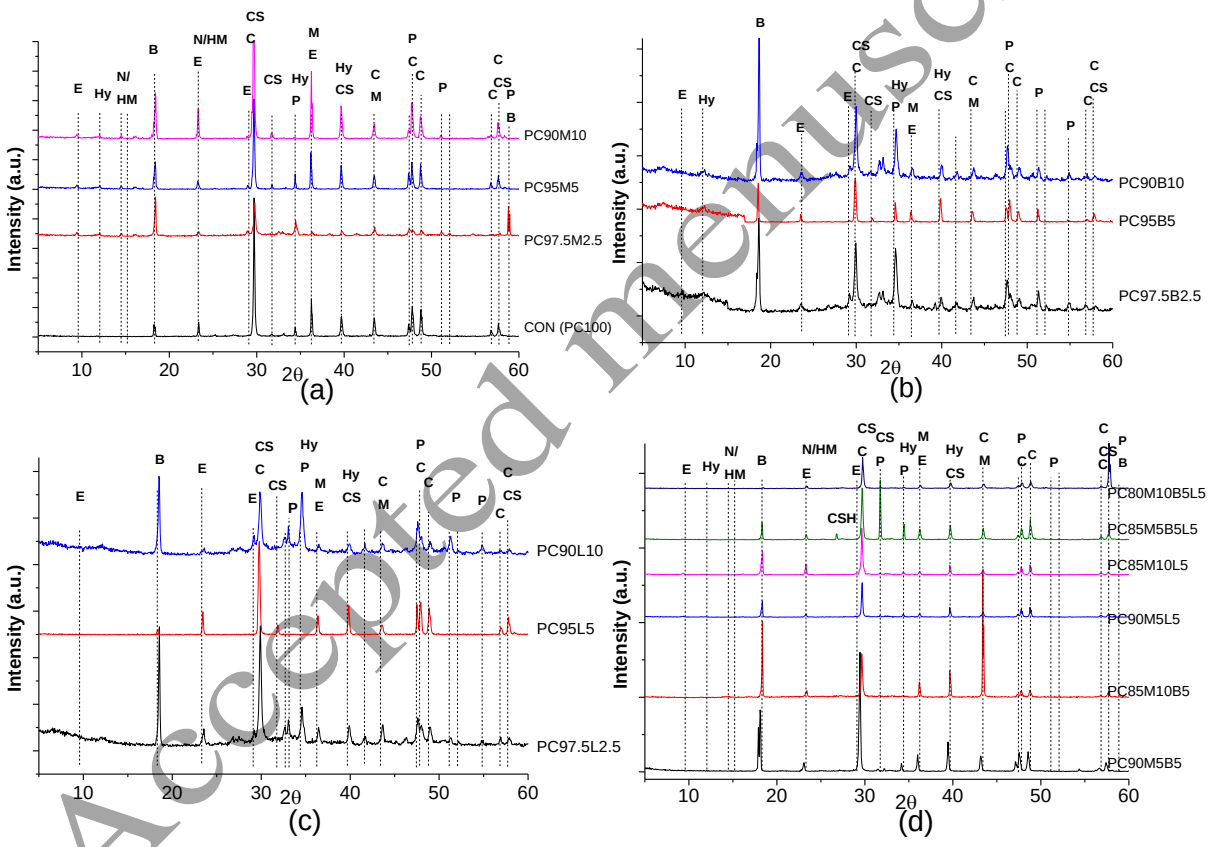

Fig.11. XRD spectra of self-healing materials, (a) CON and MgO-mixes, (b) bentonite-mixes, (c) lime-mixes, and (d) combination, (Graph notations: E= Ettringite, Hy= Hydrotalcite, N/HM= Nesquehonite/Hydromagnesite, B=Brucite, C= Calcite, CS= C_2S and C_3S, P= Portlandite, M=MgO/$MgCO_3$).

The intensity of healing compounds for calcite, portlandite/brucite and ettringite peaks were considerably sharper (Fig. 11) compared to initial (one day hydrated) cement mixes (Fig. 9). Primary

PC hydrated clinker product C-S-H gel was not identified due to its amorphous nature. Then again ordered C-S-H tobermorite/gennite-type phases was indicated in all mixes around 27^{o} and 30^{o} (2θ). Also, anhydrite peaks diminishes in the healing materials XRD graphs.

Substitutions of expansive minerals have produced additional hydrated and carbonated healing products along with the typical healing compounds. Magnesium oxide has improved the production of brucite and different hydromagnesite phases. Associated peaks for the MgO hydration products showed an increasing trend with the increase of MgO proportion in the mix (Fig. 11a). Similarly, quicklime and bentonite improved the formation of portlandite and ettringite in the healing compound. Combined minerals have combined impact on the healing compound formation characteristics. Magnesian calcite and dolomite peaks were also identified in mixes containing reactive MgO. However, calcite and magnesian calcite peak patterns were similar, making it difficult to distinguish each other.

3.4.2 TGA of healing materials

The comparative TGA curves of healing products are presented in Fig. 12. The TGA curves pattern and intensity of healing products are different compared to initial mixes, although DTG curves indicated major weight loss for similar products. TGA weight loss pattern in the healing materials commonly corresponds to ettringite, C-S-H, brucite, calcium hydroxide (CH), and carbonate phases.

A quantification of TGA weight loss (non-evaporative water loss) percentage between three major ranges associated to brucite: 300 – 400^{o}C, CH: 400 – 500^{o}C, and carbonate phases (CP): 600 – 750^{o}C, was measured and plotted in Fig. 12e as similarly presented in Fig. 10e for initial mixes. The weight loss percentages are higher in healing materials compared to the initial cement mixes. One of the major healing product ettringite presences is indicated with sharp DTG intensity at ~68^{o}C in all mixes. However, quantification at this low TGA temperature would not be accurate thus it was not considered in quantification. The increasing proportions of MgO resulted in higher proportions of brucite and the formation of associated products in all MgO mixes (Fig. 12 a, d and e). The TGA weight loss for brucite in 2.5, 5 and 10% MgO substitution mixes (Fig. 12e) gradually increases to 1.05, 1.66 and 2.28%, respectively, compared to that of 0.84% in PC100.

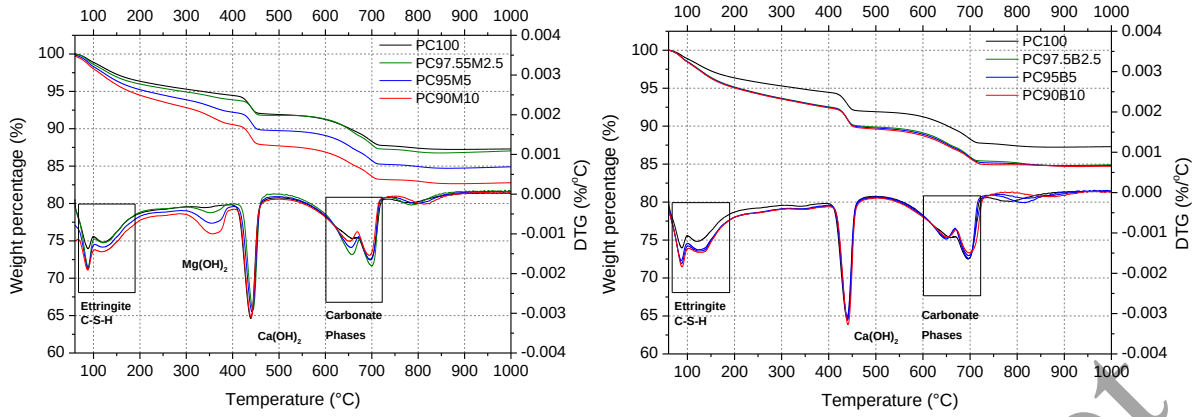

(a)

(b)

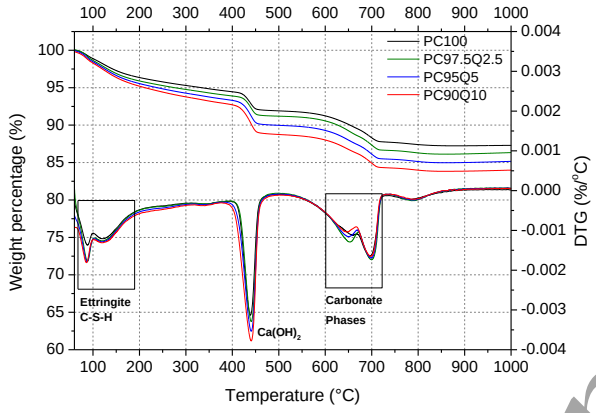

(c)

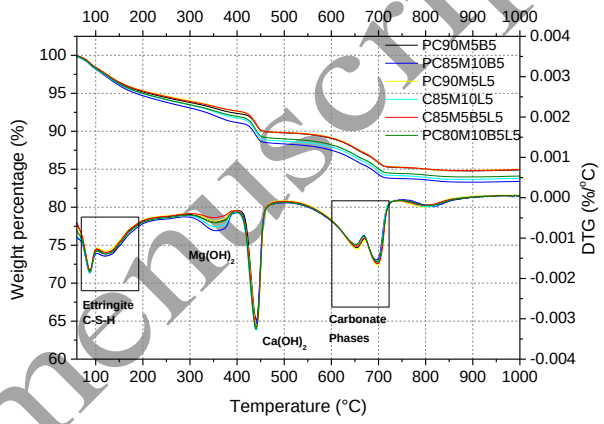

(d)

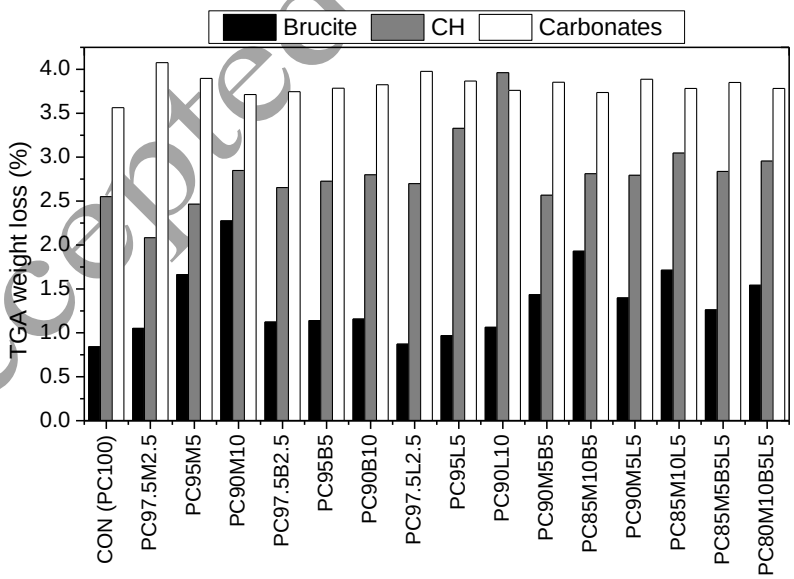

(e)

Fig.12. Comparative TGA curves of healing materials, (a) CON and MgO-mixes, (b) CON and bentonite-mixes, (c) CON and quicklime-mixes, (d) combination mixes, and (e) TGA weight loss (%) for brucite, CH, and carbonate phases.

MgO in the initial cement mix remained considerably unhydrated which hydrated during the healing process producing higher content of healing products. Bentonite mixes also showed an increasing trend in the weight loss compared to PC100, although increasing bentonite in mix proportions not showed much difference. Quicklime showed increasing mass loss trend for CH with the increasing mix proportions (Fig. 12c and e). The TGA weight loss for CH in 2.5, 5 and 10% quicklime substitution mixes (Fig. 12e) gradually increases to 2.70, 3.33 and 3.96%, respectively, compared to that of 2.55% in PC100. Even though, a portion of quicklime was hydrated in the initial mixes, a considerable proportions remained hydrated influencing the production of higher content of CH to trigger the self-healing process.

Combined minerals have combined impact on the TGA curves. Carbonates such as calcite are primary self-healing product in all mixes. Both 2.5% MgO and quicklime mixes resulted in higher carbonate production in healing compounds. However, increasing both MgO and quicklime increased the production of their primary healing hydration products which are brucite and portlandite (CH), respectively. In fact, TGA weight loss for CH in PC90M10 mix is higher than carbonate phase (Fig. 12e). This is unlike the initial cement mixes TGA results. Healing products of mineral substitution mixes were more hydrated compared to the PC100 mix. This may explain the higher strength recovery nature of mineral containing mixes.

3.4.3 SEM image and quantitative EDX analysis on healing materials

Microstructural imaging and a quantitative elemental composition are measured to have a further understanding of the formation of healing compounds and self-healing results. Typical healed surface SEM micrographs of each mix are presented in Fig. 13. Common healing products were calcite, portlandite, ettringite, and C-S-H in all mixes which are in agreement with XRD and TGA results. The microstructural morphology of the healing products were clearly visualised, and their corresponding atomic mass composition also showed similar trends.

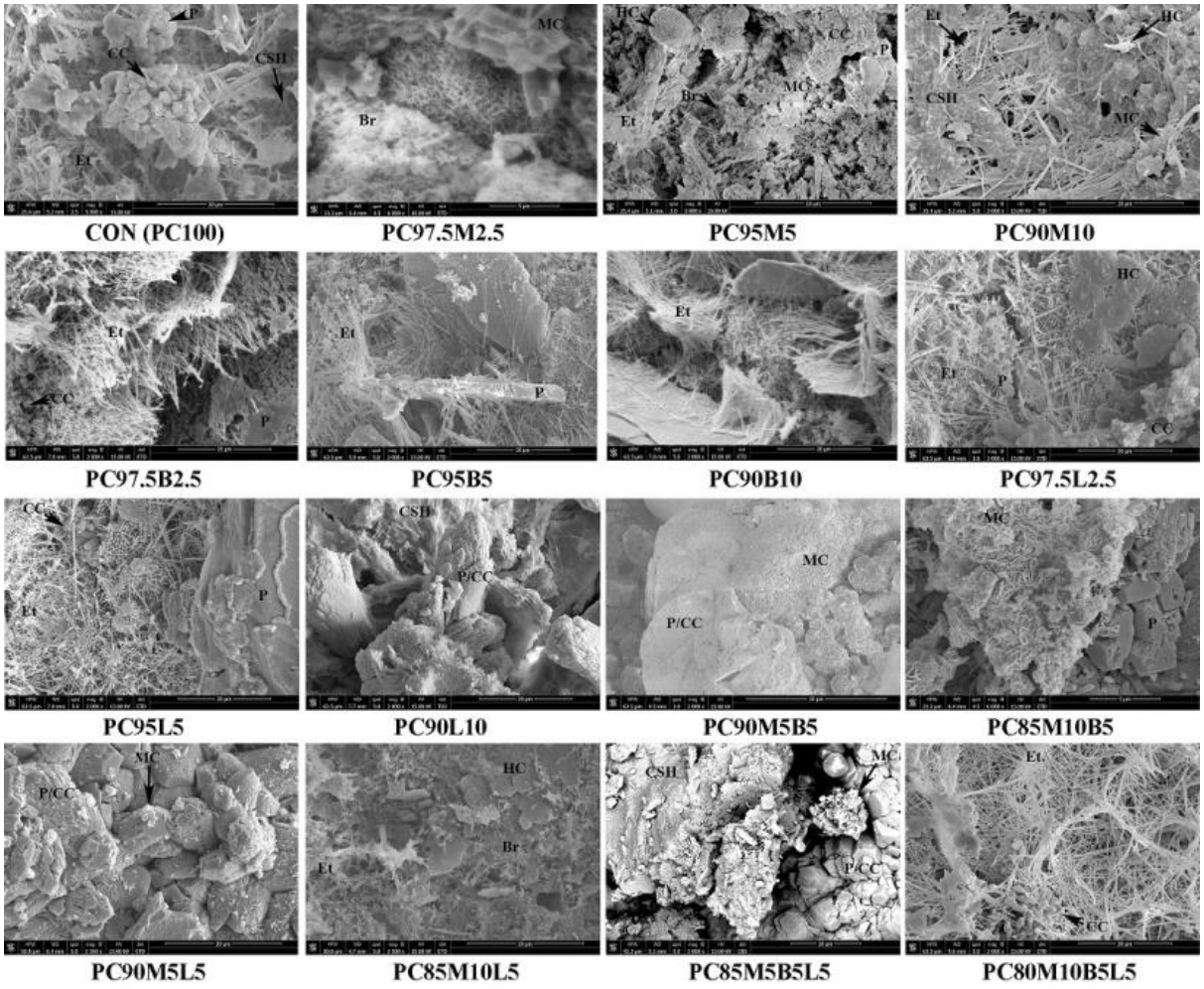

Fig. 13. Typical SEM micrograph images of the healed surface (Notations: B=Brucite, CC= Calcite, CSH = C-S-H, Et= Ettringite, HC= Hemi-carbonates, MC= Magnesium carbonates, and P= Portlandite).

Two sets of ternary diagrams, Ca-Mg-Si and Ca-Al-Si, are illustrated in Fig. 14 and Fig. 15 based on the EDX atomic mass proportions normalised values. These diagrams schematically represent the materials phase relations. To approach the mineralogy, few known Mg-containing minerals were also plotted in Fig. 14d. The atomic mass percentage of akermanite, monticellite, diopside, merwinite, and bredigite, were collected from the literature [60]. Both sets of ternary diagrams indicated corresponding expansive minerals influence on healing products formation. While mostly calcite and other carbonate layers were commonly found on the edge of the crack plane, a combination of hydration and carbonation products were found in-depth. The dominant proportions of calcite, portlandite, C-S-H, and ettringite were indicated in the healing materials of PC100 and quicklime mixes. The addition of MgO in the mixes has increased the production of brucite, hydromagnesite,

magnesian calcite, and M-S-H formation tendencies in healing substances. Mixes containing bentonite showed ettringite, and calcium aluminium silicon hydrate (C-A-S-H) formation tendencies and combined minerals show collective impact (Fig. 15 c and d).

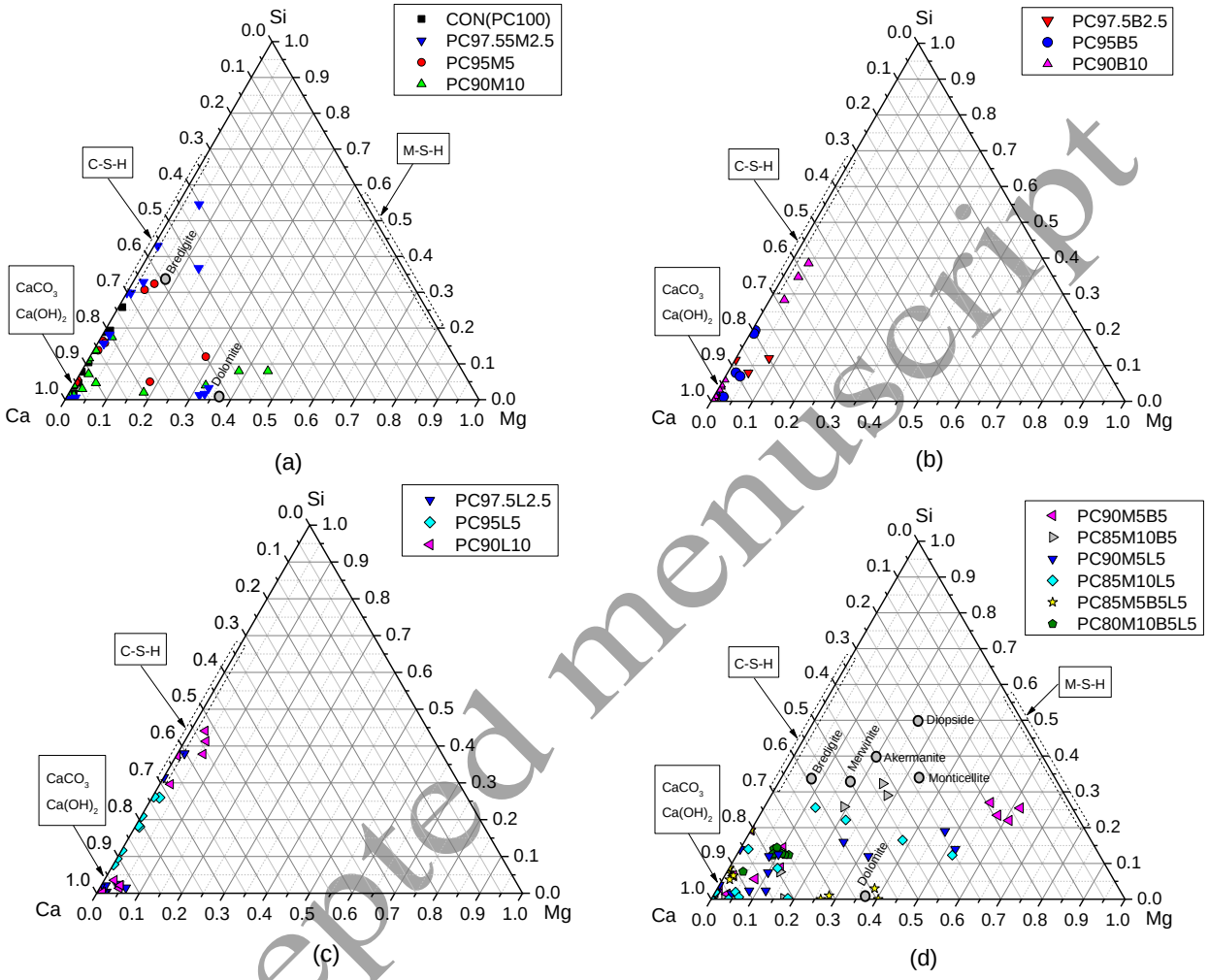

Fig. 14. Ternary diagrams of Ca-Mg-Si on healing products EDX material compositions, (a) PC100 and MgO substitution samples, (b) bentonite substitution samples, (c) quicklime substitution samples, and (d) mineral combination samples.

The production of C-S-H and portlandite autogenously triggers from the hydration of remaining unhydrated tricalcium and dicalcium silicate (C_3S and C_2S), as well as quicklime in the cement. This is now more clear that Ca^{2+} ion play the major role in the healing products formation. While this Ca^{2+} in the crack plane is supplied by the unhydrated C_3S, C_2S phases and additive quicklime, literature suggests that Ca^{2+} could be further provided by the decalcification of portlandite, C-S-H gel, and

ettringite [61,62]. The C-S-H layers were preferably found in the core zone of the healed cross-section since the ingress of dissolved CO_2 through crack reduced due to the outer layer calcite formation (Fig. 4). Calcite and portlandite in the cracks might further react with Ca-rich mono sulphate and formed ettringite and hemi-carbonates for self-healing as can be noted in several SEM images (e.g. PC95M5 in Fig. 13).

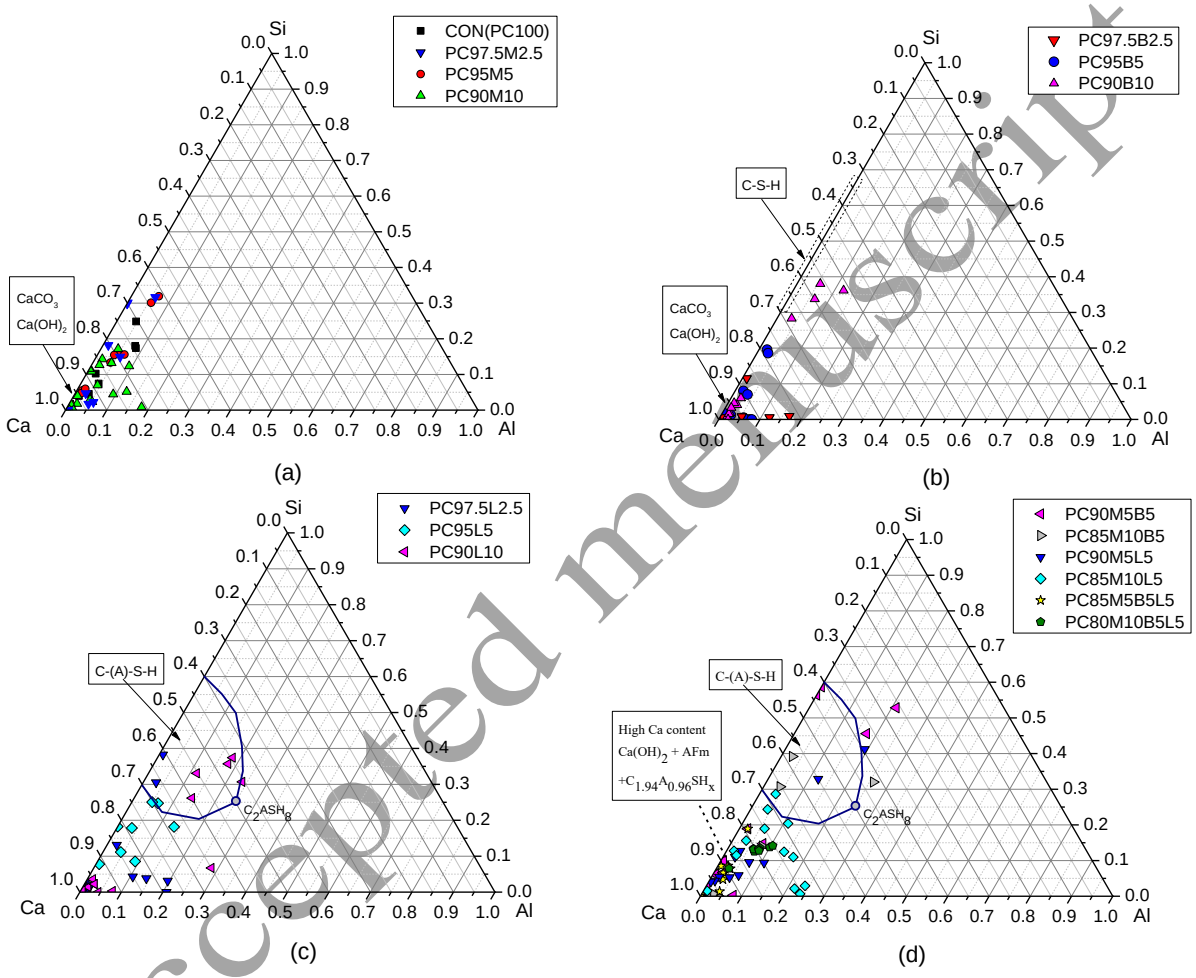

Fig. 15. Ternary diagrams of Ca-Al-Si on healing products EDX material compositions, (a) PC100 and MgO substitution samples, (b) bentonite substitution samples, (c) quicklime substitution samples, and (d) mineral combination samples.

Magnesium oxide in the mixes produced magnesium based hydrated products. The relatively lower hydration rate of MgO compared to CaO and cement-pozzolan might have limited the hydration and carbonation rate of MgO in early hydration stages. This is obviously depends on the specific grade of reactive MgO, which in this study was moderately reactive grade with the acidic reactivity of 149 sec.

The faster formation of a dense Ca-bearing carbonate layers around MgO might influence the diffusion of Mg^{2+} ions thus creating intact Mg^{2+} prone zones around the MgO and $Mg(OH)_2$ surface [63–65]. Hence, Mg^{2+} ions were found available on the crack surface, which increases the efficiency of healing products formation. The XRD and TGA on the initial cement mix after one-day hydration confirmed the presence of considerable unhydrated MgO (Fig.9 and Fig.10). This remaining unhydrated MgO may lead towards the formation of primary hydration products such as $Mg(OH)_2$ and $MgCO_3.3H_2O$ as found in SEM images (e.g. PC97.5M2.5 in Fig. 13). There is also an indication of magnesian calcite formation where calcium and magnesium carbonate microstructure found with each other (e.g. PC90M5B5 in Fig. 13).

As revealed by SEM imaging, bentonite might have assisted in the formation of scaffolding-like ettringite networks and its characteristics plane sheet layered microstructure in the crack plane. Although individually bentonite mixes demonstrated limited improvement in healing performance, this improves while bentonite combined with MgO and quicklime.

Overal microstructural observation coincided with the self-healing performances of different mixes. Therefore initially an ettringite type and layered rehydrated microstructural network may have formed, and other hydrating and carbonating compounds then started to integrate into the network filling the gaps. This creates strong bonding materials between crack surfaces and heals it.

4. Conclusions

This paper reports the early age autogenous healing capacity of cement mixes with three expansive minerals, magnesium oxide (MgO), bentonite clay and quicklime. The following conclusions can be drawn:

- The hydration of un-hydrated cementing and expansive minerals initiated the recovery of flexural strength, sealing of the cracks, and reduction in gas permeability.
- The strength recovery and crack sealing efficiency in the expansive mineral containing cement mixes improved up to 60% and 95% respectively compared to that of 8% and 56% in the 100% PC cement mix CON (PC100).

- The gas permeability coefficient decreased up to 69% in the mineral containing mixes compared to PC100. This is an indication of durability improvement due to the substitution of expansive minerals.
- Microstructural investigation on initial cement mixes confirms the presence of both hydrated and a considerable proportion of unhydrated phases of expansive minerals in the cement matrix. This has increased the autogenous healing capacity of different mixes.
- Although higher water to cement ratio was supposed to reduce the healing capacity, the supplementary expansive minerals compensate this and further improved healing.
- Common healing compounds were calcite, portlandite, ettringite, and C-S-H. Magnesium oxide encouraged in the formation of brucite, other magnesium hydro-carbonate products. Bentonite influenced in the formation of ettringite and layered microstructures. Quicklime influenced additional portlandite, calcite and calcium-based hydration products.
- Efficient healing performance was noted in 5% individual mineral substitution mixes, 5% both MgO and bentonite (PC90M5B5) mix, and 5% each mineral combined (PC85M5B5L5) mix. Follow through this, Part-II presents further optimisation in mix proportions and cracking age impact on healing process.

Acknowledgement

The support of Islamic Development Bank (IDB) scholarship collaborating with Cambridge Overseas Trust for the first author's PhD research is greatly appreciated. Moreover, collaboration from the Engineering and Physical Sciences Research Council (EPSRC) for this study (Project Ref. EP/K026631/1 – *"Materials for Life: Biomimetic multi-scale damage immunity for construction materials"*) is also gratefully acknowledged.

Reference

[1] G.C. Gifford, National Structural Concrete Specifi cation for Building Construction, 4th Editio, 2009.

[2] K. Lauer, F. Slate, Autogenous Healing of Cement Paste, ACI J. Proc. 52 (1956) 1083–1098. doi:10.14359/11661.

[3] R.K. Dhir, C.M. Sangha, J.G.L. Munday, Strength and Deformation Properties of Autogenously Healed Mortars, J. Am. Concr. Inst. 70 (1973) 231–236. doi:10.14359/11202.

[4] E.F. Wagner, Autogenous healing of cracks in cement-mortar linings for gray-iron and ductile-iron water pipe, Am. Water Work. Assoc. 66 (1974) 358–360.

[5] C. Edvardsen, Water permeability and autogeneous healing of cracks in concrete, ACI Mater. J. 96 (1999) 448–454. doi:10.14359/645.

[6] W. Ramm, M. Biscoping, Autogenous healing and reinforcement corrosion of water-penetrated separation cracks in reinforced concrete, Nucl. Eng. Des. 179 (1998) 191–200. doi:10.1016/S0029-5493(97)00266-5.

[7] H.-W. Reinhardt, M. Jooss, Permeability and self-healing of cracked concrete as a function of temperature and crack width, Cem. Concr. Res. 33 (2003) 981–985. doi:10.1016/S0008-8846(02)01099-2.

[8] M. Rooij, K. van Tittelboom, N. Belie, E. Schlangen, Self-Healing Phenomena in Cement-Based Materials: State-of-the-Art Report of RILEM Technical Committee, Springer, 2013. doi:10.1007/978-94-007-6624-2.

[9] V.C. Li, Y.M. Lim, Y.-W. Chan, Feasibility study of a passive smart self-healing cementitious composite, Compos. Part B Eng. 29 (1998) 819–827. doi:10.1016/S1359-8368(98)00034-1.

[10] C. Dry, Matrix cracking repair and filling using active and passive modes for smart timed release of chemicals from fibers into cement matrices, Smart Mater. Struct. 3 (1994) 118–123. doi:10.1088/0964-1726/3/2/006.

[11] C.M. Dry, Design of self-growing, self-sensing, and self-repairing materials for engineering applications, in: A.R. Wilson, H. Asanuma (Eds.), Proc. SPIE - Int. Soc. Opt. Eng., 2001: pp. 23–29. doi:10.1117/12.424430.

[12] Z. Yang, J. Hollar, X. He, X. Shi, A self-healing cementitious composite using oil core/silica gel shell microcapsules, Cem. Concr. Compos. 33 (2011) 506–512. doi:10.1016/j.cemconcomp.2011.01.010.

[13] J.Y. Wang, H. Soens, W. Verstraete, N. De Belie, Self-healing concrete by use of microencapsulated bacterial spores, Cem. Concr. Res. 56 (2014) 139–152. doi:10.1016/j.cemconres.2013.11.009.

[14] S. Qian, J. Zhou, M.R. de Rooij, E. Schlangen, G. Ye, K. van Breugel, Self-healing behavior of strain hardening cementitious composites incorporating local waste materials, Cem. Concr. Compos. 31 (2009) 613–621. doi:10.1016/j.cemconcomp.2009.03.003.

[15] Z.H. Zhou, Z.Q. Li, D.Y. Xu, J.H. Yu, Influence of Slag and Fly Ash on the Self-Healing Ability of Concrete, Adv. Mater. Res. 306-307 (2011) 1020–1023. doi:10.4028/www.scientific.net/AMR.306-307.1020.

[16] J. Qiu, H.S. Tan, E.-H. Yang, Coupled effects of crack width, slag content, and conditioning alkalinity on autogenous healing of engineered cementitious composites, Cem. Concr. Compos. 73 (2016) 203–212. doi:10.1016/j.cemconcomp.2016.07.013.

[17] K. Olivier, Experimental studies of self-healing cementitious materials incorporating mineral admixtures, Proc. Fourth Int. Coferene Self Heal. Mater. CD (2013) 21–24. http://repository.tudelft.nl/view/conferencepapers/uuid:51d7c62b-b51c-4965-982d-d37951f826ab/ (accessed May 30, 2015).

[18] T.-H. Ahn, T. Kishi, Crack Self-healing Behavior of Cementitious Composites Incorporating Various Mineral Admixtures, J. Adv. Concr. Technol. 8 (2010) 171–186. doi:10.3151/jact.8.171.

[19] A. Hosoda, S. Komatsu, T. Ahn, T. Kishi, S. Ikeno, K. Kobayashi, Self healing properties with various crack widths under continuous water leakage, Concr. Repair, Rehabil. Retrofit. II. (2009) 221–227. http://dicata.ing.unibs.it/plizzari/CD/Pdf/028.pdf.

[20] K. Sisomphon, O. Copuroglu, E. a. B. Koenders, Self-healing of surface cracks in mortars with expansive additive and crystalline additive, Cem. Concr. Compos. 34 (2012) 566–574. doi:10.1016/j.cemconcomp.2012.01.005.

[21] Z. Jiang, W. Li, Z. Yuan, Influence of mineral additives and environmental conditions on the self-healing capabilities of cementitious materials, Cem. Concr. Compos. 57 (2015) 116–127. doi:10.1016/j.cemconcomp.2014.11.014.

[22] Jaroenratanapirom, Dechkhachorn, R. Sahamitmongkol, Effects of different mineral additives and cracking ages on self-healing performance of mortar, Proc. 6th Annu. Concr. Conf. Petchaburi, Thailand. (2010). http://kmcenter.rid.go.th/kcresearch/article_out/article_066 OUT_T.pdf.

[23] P. Termkhajornkit, T. Nawa, Y. Yamashiro, T. Saito, Self-healing ability of fly ash-cement systems, Cem. Concr. Compos. 31 (2009) 195–203. doi:10.1016/j.cemconcomp.2008.12.009.

[24] T. Watanabe, Y. Fujiwara, C. Hashimoto, K. Ishimaru, Evaluation of Self Healing Effect in Fly-Ash Concrete By Ultrasonic Test Method, Int. J. Mod. Phys. B. 25 (2011) 4307–4310. doi:10.1142/S0217979211066830.

[25] K. Van Tittelboom, E. Gruyaert, H. Rahier, N. De Belie, Influence of mix composition on the extent of autogenous crack healing by continued hydration or calcium carbonate formation, Constr. Build. Mater. 37 (2012) 349–359. doi:10.1016/j.conbuildmat.2012.07.026.

[26] H. Huang, G. Ye, D. Damidot, Effect of blast furnace slag on self-healing of microcracks in cementitious materials, Cem. Concr. Res. 60 (2014) 68–82. doi:10.1016/j.cemconres.2014.03.010.

[27] S. Valcke, M. de Rooij, T. Nijland, H. Fisher, S. Mendoza, Carriers of self- healing agents in concrete and their effect on the microstructure, 2009.

[28] S.Z. Qian, J. Zhou, E. Schlangen, Influence of curing condition and precracking time on the self-healing behavior of Engineered Cementitious Composites, Cem. Concr. Compos. 32 (2010) 686–693. doi:10.1016/j.cemconcomp.2010.07.015.

[29] S.K. Antiohos, A. Papageorgiou, V.G. Papadakis, S. Tsimas, Influence of quicklime addition on the mechanical properties and hydration degree of blended cements containing different fly ashes, Constr. Build. Mater. 22 (2008) 1191–1200. doi:10.1016/j.conbuildmat.2007.02.001.

[30] K. Sisomphon, O. Copuroglu, A. Fraaij, Application of encapsulated lightweight aggregate impregnated with sodium monofluorophosphate as a self-healing agent in blast furnace slag mortar, Heron. 56 (2011) 17–36. http://repository.tudelft.nl/view/ir/uuid:989836d6-dd5c-4bb0-8d9f-925390dddbae/.

[31] Y.-S. Lee, J.-S. Ryou, Self healing behavior for crack closing of expansive agent via granulation/film coating method, Constr. Build. Mater. 71 (2014) 188–193. doi:10.1016/j.conbuildmat.2014.08.045.

[32] L. Ferrara, V. Krelani, F. Moretti, On the use of crystalline admixtures in cement based construction materials: from porosity reducers to promoters of self healing, Smart Mater. Struct. 25 (2016) 084002. doi:10.1088/0964-1726/25/8/084002.

[33] T.S. Qureshi, A. Al-Tabbaa, Self-healing of drying shrinkage cracks in cement-based materials incorporating reactive MgO, Smart Mater. Struct. 25 (2016) 084004. doi:10.1088/0964-1726/25/8/084004.

[34] K. Sisomphon, O. Copuroglu, E. a. B. Koenders, Effect of exposure conditions on self healing behavior of strain hardening cementitious composites incorporating various cementitious materials, Constr. Build. Mater. 42 (2013) 217–224. doi:10.1016/j.conbuildmat.2013.01.012.

[35] L. Ferrara, V. Krelani, M. Carsana, A "fracture testing" based approach to assess crack healing of concrete with and without crystalline admixtures, Constr. Build. Mater. 68 (2014) 535–551. doi:10.1016/j.conbuildmat.2014.07.008.

[36] M. Roig-Flores, S. Moscato, P. Serna, L. Ferrara, Self-healing capability of concrete with crystalline admixtures in different environments, Constr. Build. Mater. 86 (2015) 1–11. doi:10.1016/j.conbuildmat.2015.03.091.

[37] D. Palin, H.M. Jonkers, V. Wiktor, Autogenous healing of sea-water exposed mortar: Quantification through a simple and rapid permeability test, Cem. Concr. Res. 84 (2016) 1–7. doi:10.1016/j.cemconres.2016.02.011.

[38] M. Maes, D. Snoeck, N. De Belie, Chloride penetration in cracked mortar and the influence of autogenous crack healing, Constr. Build. Mater. 115 (2016) 114–124. doi:10.1016/j.conbuildmat.2016.03.180.

[39] A. Hosoda, T. Kishi, H. Arita, Y. Takakuwa, Self healing of crack and water permeability of expansive concrete, in: Proc. First Int. Conf. Self Heal. Mater., 2007: pp. 1–10.

[40] C. De Nardi, A. Cecchi, L. Ferrara, A. Benedetti, D. Cristofori, Effect of age and level of damage on the autogenous healing of lime mortars, Compos. Part B Eng. 124 (2017) 144–157. doi:10.1016/j.compositesb.2017.05.041.

[41] The influence of MgO-type expansive agent incorporated in self-healing system of Engineered cementitious Composites, Constr. Build. Mater. 149 (2017) 164–185. doi:10.1016/J.CONBUILDMAT.2017.05.109.

[42] T.S. Qureshi, A. Kanellopoulos, A. Al-Tabbaa, Encapsulation of expansive powder minerals within a concentric glass capsule system for self-healing concrete, Constr. Build. Mater. 121 (2016) 629–643. doi:10.1016/j.conbuildmat.2016.06.030.

[43] A. Kanellopoulos, T.S. Qureshi, A. Al-Tabbaa, Glass encapsulated minerals for self-healing in cement based composites, Constr. Build. Mater. 98 (2015) 780–791. doi:10.1016/j.conbuildmat.2015.08.127.

[44] F. Jin, A. Al-Tabbaa, Characterisation of different commercial reactive magnesia, Adv. Cem. Res. 26 (2014) 101–113. doi:10.1680/adcr.13.00004.

[45] BS EN 197-1, British Standard. Part I: Composition, Specifications and Conformity Criteria for Common Cements, 2011.

[46] BS EN 459-1, Building Lime: Definitions, specifications and conformity criteria, 2001.

[47] M. Shand, The chemistry and technology of magnesia, John Wiley & Sons INC., New Jersey, 2006.

[48] C.K. Chau, Z. Li, Accelerated reactivity assessment of light burnt magnesium oxide, J. Am. Ceram. Soc. 91 (2008) 1640–1645. doi:10.1111/j.1551-2916.2008.02330.x.

[49] ASTM, C 187 - 10 Standard Test Method for Normal Consistency of Hydraulic Cement Free, (2010).

[50] BS EN:196-1, Methods of testing cement. Determination of strength, Br. Stand. Inst. (2005).

[51] BS EN 12390-5, Testing hardened concrete. Flexural strength of test specimens – BSI British Standards, (2009).

[52] ASTM D790-10, Standard Test Methods for Flexural Properties of Unreinforced and Reinforced Plastics and Electrical Insulating Materials, West Conshohocken, PA, 2010.

[53] A.M. Alshamsi, H.D. a Imran, Development of a permeability apparatus for concrete and mortar, Cem. Concr. Res. 32 (2002) 923–929. doi:10.1016/S0008-8846(02)00727-5.

[54] L. Mo, M. Deng, M. Tang, Effects of calcination condition on expansion property of MgO-type expansive agent used in cement-based materials, Cem. Concr. Res. 40 (2010) 437–446. doi:10.1016/j.cemconres.2009.09.025.

[55] N. ter Heide, E. Schlangen, Selfhealing of early age cracks in concrete, Proc. First Int. Conf. Self Heal. Mater. (2007) 1–12. doi:10.1007/978-1-4020-5104-3.

[56] M.E. Bazaldúa-Medellín, A.F. Fuentes, A. Gorokhovsky, J.I. Escalante-García, Early and late hydration of supersulphated cements of blast furnace slag with fluorgypsum, Mater. Construcción. 65 (2015) e043. doi:10.3989/mc.2015.06013.

[57] H.F.W. Taylor, Cement chemistry, Thomas Telford, 1998. doi:10.1016/S0958-9465(98)00023-7.

[58] I. Natali Sora, R. Pelosato, D. Botta, G. Dotelli, Chemistry and microstructure of cement pastes admixed with organic liquids, J. Eur. Ceram. Soc. 22 (2002) 1463–1473. doi:10.1016/S0955-2219(01)00473-3.

[59] F. Jin, Characterisation and Performance of Reactive MgO-based Cements with Supplementary Cementitious Materials, University of Cambridge, 2014.

[60] L. Fernandez, C. Alonso, C. Andrade, A. Hidalgo, The role of magnesium during the hydration of C3S and C-S-H formation. Scanning electron microscopy and mid-infrared studies, Adv. Cem. Res. 17 (2005) 9–21. doi:10.1680/adcr.2005.17.1.9.

[61] C.A. García-González, A. Hidalgo, C. Andrade, M.C. Alonso, J. Fraile, A.M. López-Periago, C. Domingo, Modification of Composition and Microstructure of Portland Cement Pastes as a Result of Natural and Supercritical Carbonation Procedures, Ind. Eng. Chem. Res. 45 (2006) 4985–4992. doi:10.1021/ie0603363.

[62] P.H.R. Borges, J.O. Costa, N.B. Milestone, C.J. Lynsdale, R.E. Streatfield, Carbonation of CH and C–S–H in composite cement pastes containing high amounts of BFS, Cem. Concr. Res. 40 (2010) 284–292. doi:10.1016/j.cemconres.2009.10.020.

[63] L. Zheng, C. Xuehua, T. Mingshu, MgO-type delayed expansive cement, Cem. Concr. Res. 21 (1991) 1049–1057. doi:10.1016/0008-8846(91)90065-P.

[64] L. Mo, D.K. Panesar, Effects of accelerated carbonation on the microstructure of Portland cement pastes containing reactive MgO, Cem. Concr. Res. 42 (2012) 769–777. doi:10.1016/j.cemconres.2012.02.017.

[65] L. Mo, M. Deng, M. Tang, A. Al-Tabbaa, MgO expansive cement and concrete in China: Past, present and future, Cem. Concr. Res. 57 (2014) 1–12. doi:10.1016/j.cemconres.2013.12.007.